Progress In Electromagnetics Research M, Vol. 84, 53–62, 2019

Piezoelectric Transducer-Tuned Fourth-Order Microstrip Bandpass Filter with Cross-Coupling

Liangzu Cao[1, *], Liya Wang[2], Junmei Yan[1], and Lixia Yin[1]

Abstract—This paper presents a piezoelectric transducer-tuned fourth-order bandpass filter (BPF). The proposed filter consists of four open-loop resonators which form cascaded quadruplet (CQ) sections with a capacitive cross coupling. There are two transmission zeros (TZs) in the lower and upper stopband to further improve the selectivity of the filter. The structure parameters are optimized by using High Frequency Structure Simulator (HFSS). The piezoelectric transducer (PET) together with a dielectric substrate is used as a tuning element. The effects of the PET on the coupling coefficient and external quality factor are analyzed. The designed tunable filter has been manufactured and measured. The measured results show that the center frequency of the filter changes from 2.48 GHz to 2.28 GHz; the insertion loss basically keeps constant; 3 dB bandwidth of the filter changes from 156 MHz to 168 MHz over the tuning range; and the positions of the TZs in the stopband move synchronously as the center frequency varies.

1. INTRODUCTION

Electrically tunable filters are widely used in multiband and multi-standard communication systems. They can greatly reduce the volume, lower the design complexity of systems, and have certain advantages in reducing costs and improving reliability by replacing the traditional switched filter banks. According to the tuning elements, the electrically tunable filters can be divided into four categories: varactor-tuned filters, ferroelectric thin film filters, MEMS tunable filters, and piezoelectric-transducer (PET) tunable filters [1]. Among them, the studies on the varactor-tuned BPFs are very common due to the fast tuning speed and large capacitance ratio of the varactors. However, the obvious parasitic resistances (ESR) of the varactors result in large in-band insertion losses [2–6], and the in-band insertion losses are up to 6 dB or above for fourth-order tunable BPFs [3–6]. Therefore, many second-order varactor-tuned BPFs have been designed and published, but the selectivity of these filters is very low [7].

As mentioned above, the relatively low Q of varactor diodes restricts the implementation of higher-order and narrowband tunable filters. Fortunately, PET tunable higher-order filters have very low insertion loss over a tuning range because the PET is not directly connected to the circuit of the filter, but the published literature about PET tunable filters is sparse [8–11]. Jung et al. [8] designed a third-order hairpin PET microstrip BPF with a tuning range from 5.6 to 5.8 GHz for a control voltage from -80 to 60 V; Al-Ahmad et al. [9] manufactured a PET tunable microstrip resonator, and the resonant frequency varied from 1.1 GHz to 2.6 GHz with a voltage of 200 V applied to the PET. However, the selectivity was very low, and the bandwidth varied significantly over the wide tuning range; Hsieh and Chang [10] realized a four-stage open-loop microstrip filter tuned by a PET, and the center frequency tuning range was 126 MHz (1.874 $\sim$ 2.0 GHz) when the control voltage changed from -90 V to 90 V, but the structure was asymmetric, which increased the design complexity. We [11] studied a second-order

Received 29 May 2019, Accepted 7 August 2019, Scheduled 20 August 2019
* Corresponding author: Liangzu Cao (clz4233@aliyun.com).
[1] School of Mechanical and Electric Engineering, Jingdezhen Ceramic Institute, Jingdezhen, China. [2] Jingdezhen University, Jingdezhen, China.

PET tunable dielectric filter with a low insertion loss over the tuning range, but the tuning range was narrower.

In this paper we develop a fourth-order PET tunable microstrip BPF. A dielectric substrate is attached to the PET to widen the tuning range. A capacitive cross coupling between the first and fourth resonators is introduced to produce two TZs in the lower and higher stopbands, which further improve the filter selectivity.

2. DESIGN PROCEDURE

The performance specifications of the fourth-order tunable filter to be designed are as follows:

center frequency (f_0) range: $2.28 \sim 2.48$ GHz,

3 dB bandwidth: 200 MHz,

insertion loss: less than 2 dB,

two transmission zeros: at $f_0 \pm 500$ MHz,

poles: 4.

The coupling matrix is synthesized for the BPF with a center frequency of 2.48 GHz by using the Cameron method [12], and a 6×6 coupling matrix is obtained as follows:

$$M = \begin{array}{c} \begin{array}{cccccc} S & 1 & 2 & 3 & 4 & L \end{array} \\ \left(\begin{array}{cccccc} 0 & 1.0376 & 0 & 0 & 0 & 0 \\ 1.0376 & 0 & 0.9052 & 0 & 0.0248 & 0 \\ 0 & 0.9052 & 0 & -0.7070 & 0 & 0 \\ 0 & 0 & -0.7070 & 0 & 0.9052 & 0 \\ 0 & 0.0248 & 0 & 0.9052 & 0 & 1.0376 \\ 0 & 0 & 0 & 0 & 1.0376 & 0 \end{array} \right) \end{array} \tag{1}$$

where M_{S1} denotes the coupling between the source and the first resonator; M_{L4} denotes the coupling between the load and the fourth resonator; M_{ij} $(i \neq j)$ represents the coupling between two resonators.

It can be seen from Eq. (1) that $M_{12}(= M_{34})$ and M_{14} are positive, and M_{23} is negative. M_{14} is a cross coupling between the first and fourth resonators. Figure 1 shows the coupling topology of the filter.

In Figure 1, S and L represent a source and load, respectively; $R1, R2, R3$, and $R4$ are the first, second, third, and fourth resonators, respectively; the dark lines between two circles represent direct couplings, and the red line between $R1$ and $R4$ is a cross coupling.

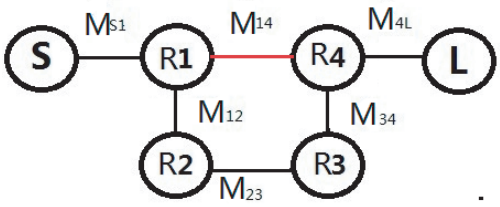

Figure 1. Coupling topology of the filter.

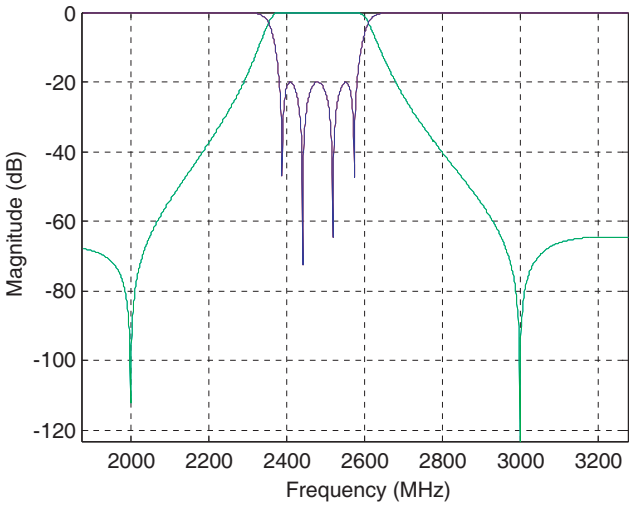

Figure 2. Response produced by a coupling matrix.

When the properties of the couplings (capacitive or inductive) accord with a certain relationship, two transmission zeros located at each side of the stopband can be produced [13]. The synthesized response is shown in Figure 2.

The coupling coefficient and external Q value corresponding to elements of the coupling matrix is calculated as follows: $k_{12} = k_{34} = 0.073$, $k_{23} = -0.057$, $k_{14} = 0.00185$, and $Q_e = 11.61$.

We design the proposed filter by using half wavelength ($1/2\lambda$) open loops which construct three different coupling structures, i.e., electrical coupling, magnetic coupling, and mixed coupling, which are useful for a BPF with cross-coupling. Figure 3 represents the structure of the proposed filter.

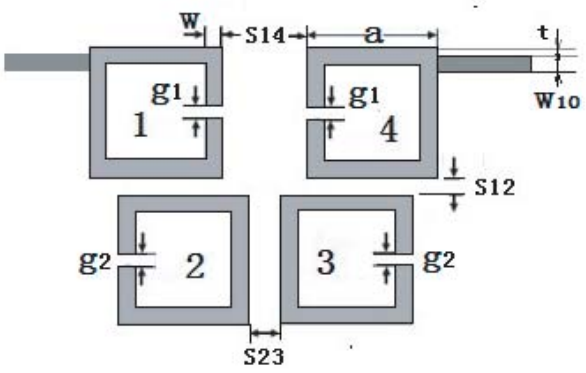

Figure 3. Structure of a fourth-order open loop bandpass filter.

In Figure 3, the numbers from 1 to 4 represent the sequentially ordered resonators. The coupling between two resonators is determined by its gap, denoted by S_{ij} $(i, j = 1 \sim 4, i \neq j)$. The input/output port is a tapped line, and the coupling is determined by the tapped position, denoted by symbol t.

The equivalent circuit of Figure 3 is shown in Figure 4. A capacitor is used to represent the electric coupling between resonators 1 and 2 or resonators 1 and 4, and an inductor is used to represent the magnetic coupling between resonators 2 and 3. TL1∼TL4 are open-circuited microstrip transmission lines of half wavelength, and Term1 and Term2 are input and output ports.

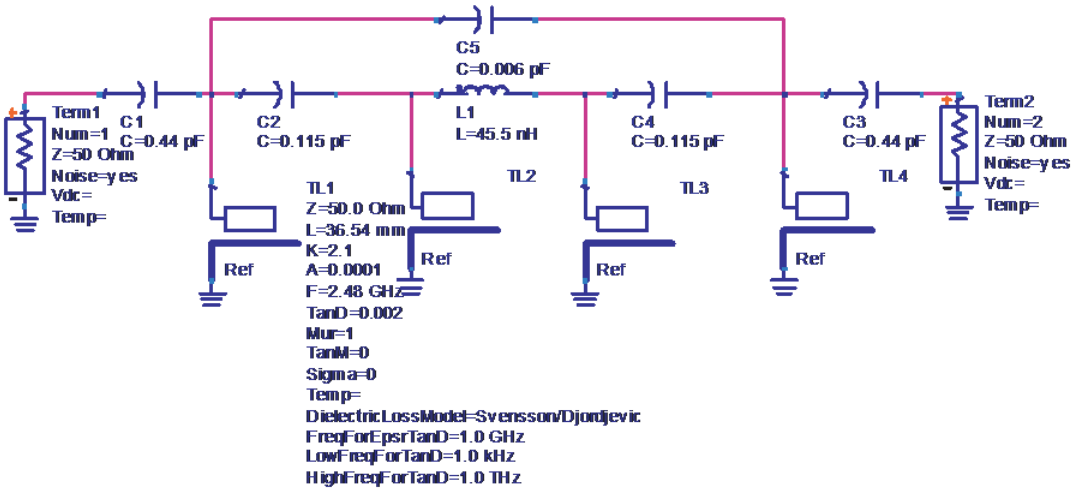

Figure 4. Equivalent circuit of the proposed filter.

We can judge the positions of TZs by using the phase shift method [13]. Table 1 shows the calculation and results of the phase shift. Below resonance and above resonance, the two paths are 180 degrees apart, which produce TZs both above and below the passband.

Table 1. Total phase shifts for two paths.

Path	Below Resonance	Above Resonance
TL1-TL2-TL3-TL4	$+90^\circ + 90^\circ - 90^\circ + 90^\circ + 90^\circ = +270^\circ$	$+90^\circ - 90^\circ - 90^\circ - 90^\circ + 90^\circ = -90^\circ$
TL1-TL4	$+90^\circ$	$+90^\circ$
Result	Out of phase	Out of phase

Figure 5 shows the simulated response by using Advanced Design System (ADS) and exhibits two transmission zeros in the higher and lower stopbands, which is consistent with that in Figure 2, and further validates the coupling properties.

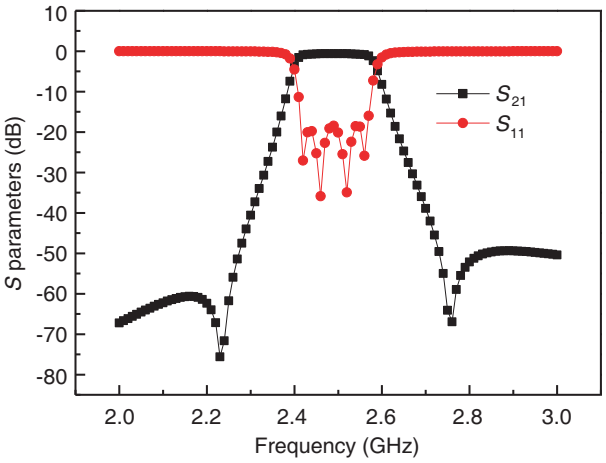

Figure 5. Simulated response of the equivalent circuit.

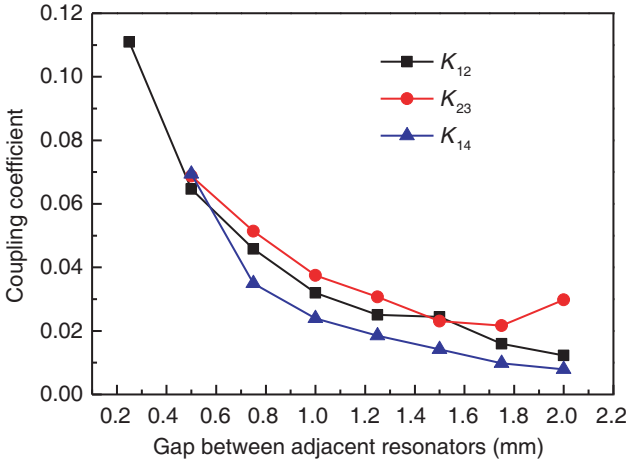

Figure 6. Coupling coefficient versa the gap between resonators.

2.1. Coupling Coefficient and External Q Value

Microstrip lines are designed on a substrate with a relative dielectric constant of 2.2 and thickness of 0.508 mm. The structure parameters are set as follows: width of open-loop line (w) of 1.5 mm, total length of 45 mm, and gap between open ends (g_1 and g_2) of 0.6 mm. Based on HFSS simulation, the coupling coefficients between two open-loop resonators are calculated by the following formula [1],

$$k_{ij} = \frac{f_e^2 - f_o^2}{f_e^2 + f_o^2} \tag{2}$$

where subscripts i and j represent the serial number of resonators, and f_e and f_o represent the even-mode and odd-mode resonant frequencies, respectively. The simulation results of coupling coefficients are shown in Figure 6.

External quality factor (Q_e) simulation adopts the method of loading on two ports, one of which is weakly coupled, and the other is the required coupling. The calculation formula is as follows [1],

$$Q_e = \frac{f_0}{\Delta f_{3\,\mathrm{dB}}} \tag{3}$$

where f_0 and $\Delta f_{3\,\mathrm{dB}}$ represent the resonant frequency and 3 dB bandwidth, respectively. External quality factor (Q_e) simulation results are shown in Figure 7.

According to the coupling coefficients and external Q values calculated by the coupling matrix, the initial structure parameters of the proposed filter can be obtained by extrapolating the curves in Figures 7 and 8, as shown in Table 2.

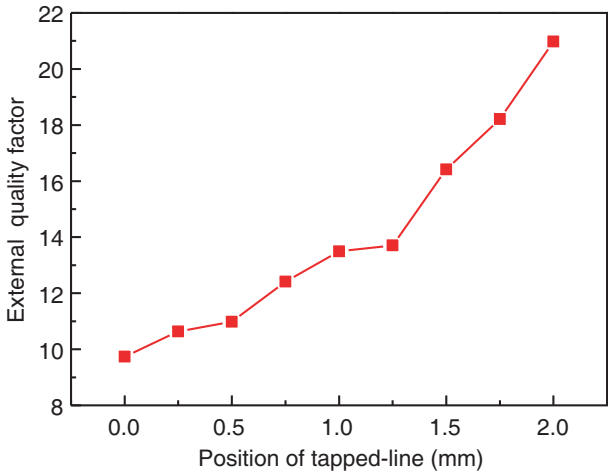

Figure 7. External quality factor versa the position of the tapped-line.

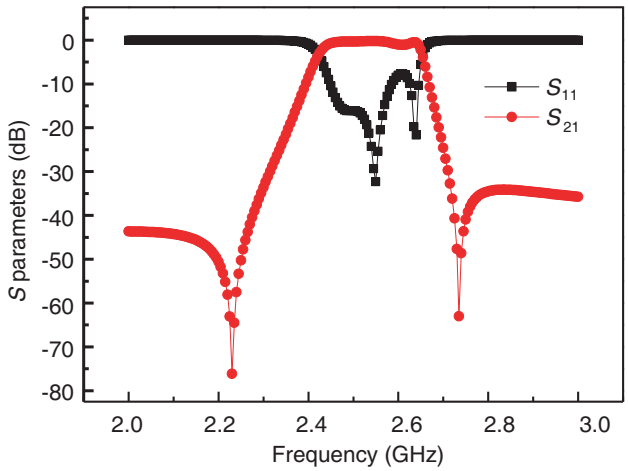

Figure 8. Initial simulated response of the proposed filter.

Table 2. Initial physical parameters of the proposed filter (unit: mm).

Parameters	$S_{12}(=S_{34})$	S_{23}	S_{14}	t
value	0.413	0.636	2.35	0.589

The simulation response based on Table 2 is shown in Figure 8 by using HFSS. There is a certain discrepancy between the simulation and requirement because the coupling between non-adjacent resonators and the effect of the coupling on each resonant frequency are ignored in the theoretical calculation.

The structure parameters of the filter can be optimized by using HFSS, and the optimized parameters are listed as follows: $S_{12}(=S_{34}) = 0.5533\,\text{mm}$, $S_{23} = 1.000\,\text{mm}$, $S_{14} = 2.8270\,\text{mm}$, $t = 0.4996\,\text{mm}$.

The optimized S parameters are shown in Figure 9. The center frequency and 3 dB bandwidth of the filter are 2.52 GHz and 148.4 MHz, respectively.

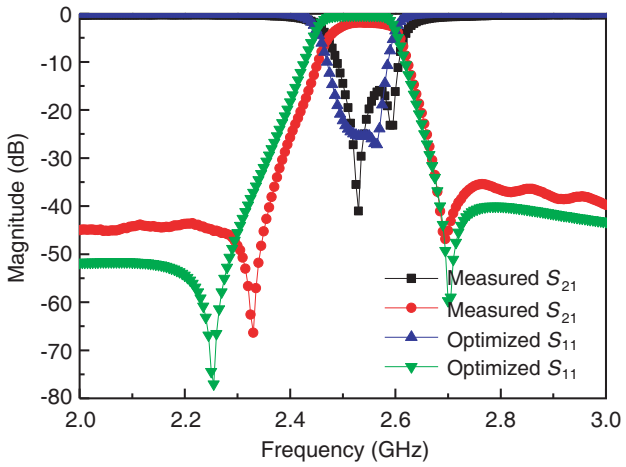

Figure 9. Optimized response of the microstrip bandpass filter with a cross coupling.

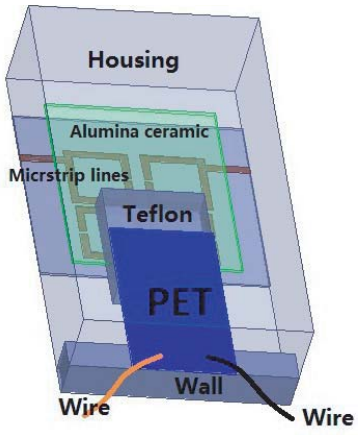

Figure 10. Configuration of piezoelectric transducer-tuned microstrip filter.

2.2. Design of the Proposed Tunable Filter

A PET is used to tune the center frequency of the proposed filter, and the structure is shown in Figure 10. One end of the PET is fixed on the wall of the housing, and the other end is adhered to a dielectric substrate (alumina ceramic substrate with a dielectric constant of 9.2 and a thickness of 0.6 mm) via a Teflon patch. The alumina ceramic substrate is called a perturber because the substrate hangs over the circuit of the filter and perturbs the electromagnetic field distributions of the microstrip lines. The PET consists of two piezoelectric layers (made of lead zirconate titanate ceramics, PZT) and a thin steel layer. The center shim laminated between the two same polarization piezoelectric layers adds mechanical strength and stiffness. The shim is connected to one polarity of a DC voltage to deflect the PET and moves it up or down vertically. As we can see from the structure in Figure 10, when the perturber moves up or down, the effective dielectric constant of the filter decreases or increases, respectively, allowing the passband of the filter to shift toward higher or lower frequency.

2.3. Effects of PET on the Coupling Coefficient and External Q Value

As the dielectric substrate moves up or down, the coupling coefficient changes accordingly, as shown in Figure 11.

As can be seen from Figure 11, the variation trends of k_{12} and k_{23} are basically the same, and the variation of k_{23} is very small. Although the variation of k_{14} is large, it controls the transmission zeros in the stopband and has less effect on the in-band characteristic.

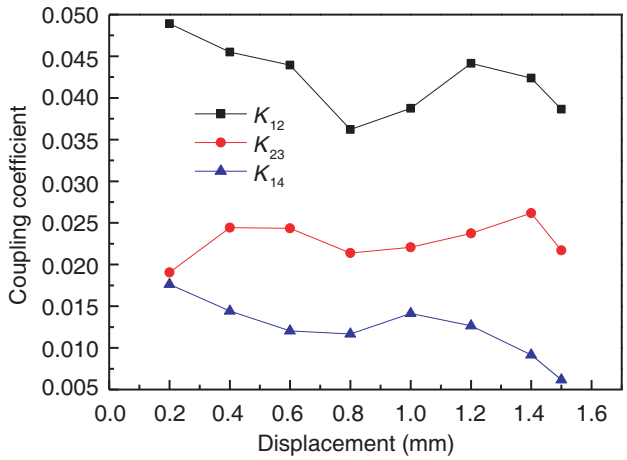

Figure 11. Coupling coefficient affected by the dielectric substrate.

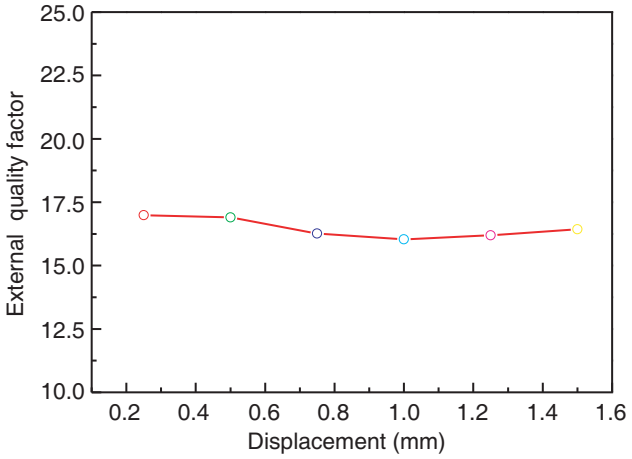

Figure 12. External quality factor affected by the dielectric substrate.

Figure 12 shows the effect of the dielectric substrate on the external quality factor. It can be observed that the external quality factor is unchanged.

2.4. Effects of PET on the Performances of the Filter

The distance between the bottom of the dielectric substrate and the surface of the filter is denoted by a symbol h, and the effects of PET on the performance of the filter are displayed in Figure 13. The center frequency of the filter changes from 2.50 GHz to 2.475 GHz, and 3 dB bandwidth of the filter varies from 145.8 MHz to 140.4 MHz when h is decreased from 1.5 mm to 0.5 mm. The in-band reflection loss of the filter is more than 10 dB. Compared to the case without dielectric substrate, the center frequency of the filter tuned by PET is lowered due to the dielectric substrate increasing the effective dielectric constant of the microstrip lines.

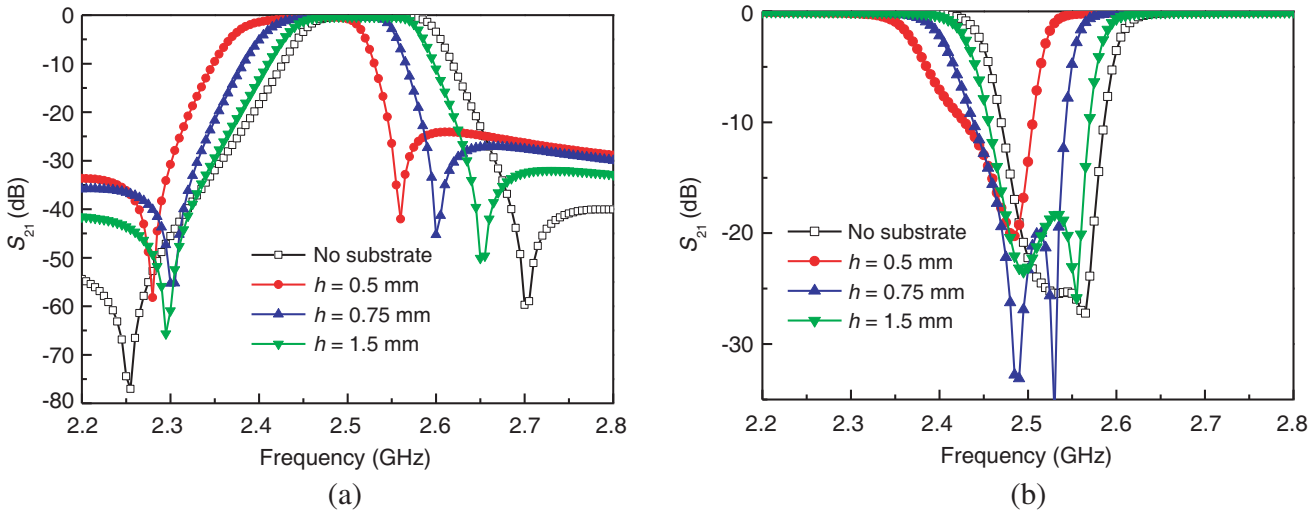

Figure 13. The performances of the filter affected by the dielectric substrate. (a) Transmission responses. (b) Reflection responses.

3. EXPERIMENTS AND RESULTS

The proposed filter is made on a Rogers 5880 dielectric substrate with a relative dielectric constant of 2.2, dissipation factor ($\tan\delta$) of 9×10^{-4}, and thickness of 0.508 mm, and installed within an aluminum housing. Before being tuned by PET, the microstrip filter is measured by using a vector network analyzer Agilent E5071B through SMA connectors, and the measured result is plotted in Figure 9. It can be seen that the in-band insertion loss is larger than that of the simulated one due to the conductance loss of metal layers and the dielectric loss of the substrate, and the measured in-band bandwidth is slightly less than that of the simulated one due to the processing tolerance. A PET (including a Teflon patch and an alumina substrate) is fixed on the wall of the housing, and the sizes and performances of the PET are listed in Table 3. The fabricated filter is measured, and a photo of the filter is shown in Figure 14.

When the voltage applied to the PET changes from 0 V to 50 V, the frequency responses of the filter are plotted in Figure 15.

The measured results show that the center frequency of the filter is tuned from 2.48 GHz to 2.28 GHz

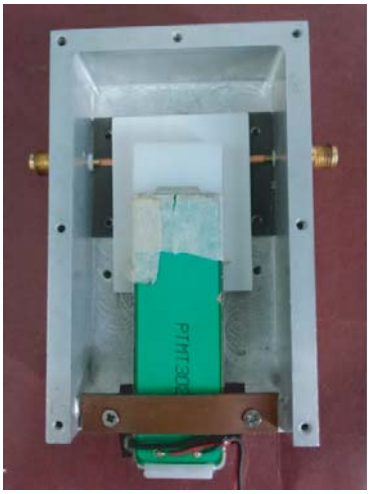

Figure 14. Photo of the fabricated tunable filter.

Table 3. Mechanical and electrical performances.

Dimensions $L \times W \times t$	Deflection	Block force	Leakage current	Capacitance
[mm]	[mm]	[mN]	[μA]	[nF@1 V, 100 Hz]
$60 \times 20 \times 0.6$	$\geqq 0.8$	$\geqq 300$	$\leqq 10$	300

(the tuning range of 200 MHz); the in-band insertion loss varies from 1.52 dB to 1.88 dB (the variation less than 0.36 dB); the 3 dB bandwidth changes from 168 MHz to 156 MHz; and the in-band reflection loss is more than 10 dB. There are two TZs in the lower and upper stopbands. The attenuation of the lower TZ is greater than 55 dB, and that of the upper one is greater than 45 dB.

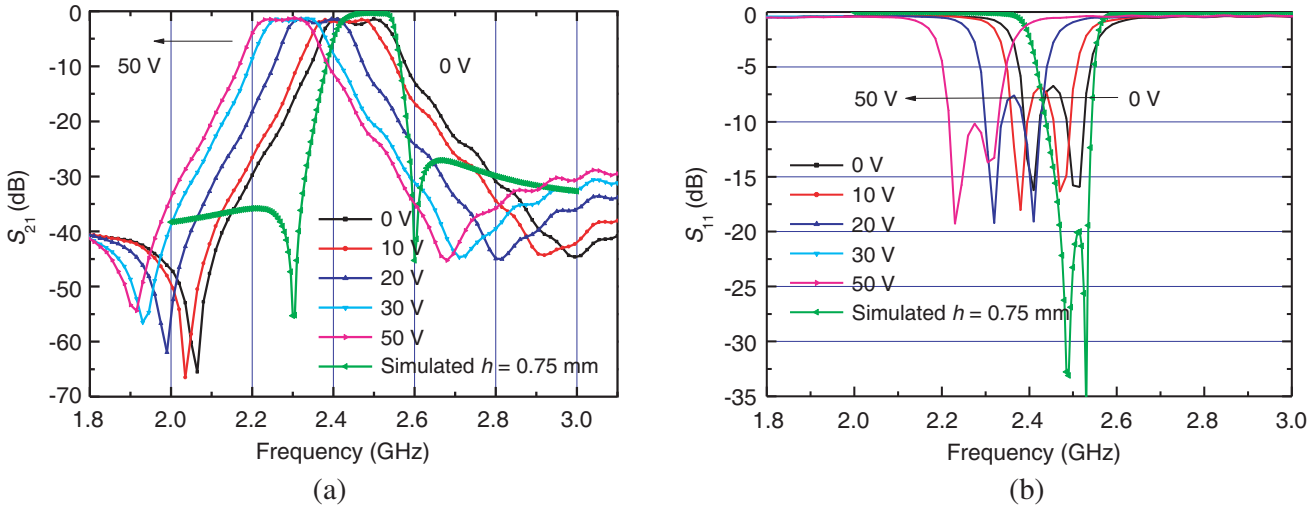

Figure 15. Frequency responses of the proposed tunable filter. (a) Transmission responses. (b) Reflection responses.

Table 4. Comparison of the performances of the tunable filters.

Number	Tuning range (GHz)	Bandwidth (MHz or %)	Insertion loss (dB)	Order	TZ	Tuning element	Control voltage (V)
[3]	0.76–1.08	10%	$6.0 \sim 3.5$	4	no	varactor	$0 \sim 12$ ($V_1 \sim V_4$)
[4]	$1.17 \sim 1.37$	$37 \sim 77$	$6.3 \sim 2.3$	4	no	varactor	$1 \sim 30$ (V_1)
[5]	1.5–2.1	80 ± 10	$6.0 \sim 4.5$	4	two	varactor	$0.7 \sim 6$ ($V_1 \sim V_4$)
[6]	$0.79 \sim 1.31$	74 ± 15	$6.6 \sim 5.9$	4	no	varactor	$1 \sim 30$ ($V_1 \sim V_2$)
[8]	$5.6 \sim 5.8$	0.414%	2.7	3	no	PET	$-80 \sim 60$
[9]	$1.1 \sim 2.6$	Large variation	$2 \sim 4$	1	no	PET	$0 \sim 200$
[10]	$1.874 \sim 2.0$	130 (at 0 V)	2.75	4	two	PET	$-90 \sim 90$
[11]	$4.15 \sim 4.20$	$37 \sim 40$	$1 \sim 1.7$	2	no	PET	$0 \sim 50$
This work	2.28–2.48	$156 \sim 168$	$1.52 \sim 1.88$	4	two	PET	$0 \sim 50$

One state of the measured responses (at 0 V) is compared with the simulated one with $h = 0.75$ mm for clearness, and it is seen that the two do not agree with each other because we cannot find the precise relationship between the displacement of the PET and the DC voltage applied to the PET. In fact, the movement of the PET together with the substrate is more complicated than a rather simple upward or downward movement under the control of a DC voltage.

Table 4 compares the measured results of this work with the literature. It can be seen from the table that both the in-band insertion loss and its variation in the tuning range are smaller, and the selectivity is better than that of the filters in the literature.

4. CONCLUSION

A fourth-order bandpass filter is designed by using microstrip open-loop resonators. A cross coupling is introduced between the first and fourth resonators, and two transmission zeros are produced on both sides of the stopband of the filter to further improve the selectivity of the filter. A piezoelectric transducer together with a dielectric substrate has little effect on the coupling coefficients and external factor, which keeps the filter's responses unchanged during the tuning operation. The measured results show that the 3 dB bandwidth and insertion loss of the proposed filter change little over the tuning range (from 2.28 GHz to 2.48 GHz), and the two transmission zeros of the filter move with the center frequency to maintain the selectivity of the filter. The measured results are compared with those of the literature, and some performances are better than those of the literature.

ACKNOWLEDGMENT

This work was supported by the National Natural Science Foundation of China (61661023), PhD research startup foundation of Jingdezhen Ceramic Institute of China (2018-01) and the Jingdezhen science and Technology Bureau (20182GYZD011-18).

REFERENCES

1. Hong, J.-S., *Microstrip Filters for RF/Microwave Applications*, Wiley, New York, NY, USA, 2011.
2. Schuster, C., A. Wiens, F. Schmidt, et al., "Performance analysis of reconfigurable bandpass filters with continuously tunable center frequency and bandwidth," *IEEE Transactions on Microwave Theory and Techniques*, Vol. 65, No. 11, 4573–4584, 2017.
3. Cho, Y.-H. and G. M. Rebeiz, "Two- and four-pole tunable 0.7–1.1-GHz bandpass-to-bandstop filters with bandwidth control," *IEEE Transactions on Microwave Theory and Techniques*, Vol. 62, No. 3, 457–463, 2014.
4. Hao, S. and Q. J. Gu, "A Fourth order tunable capacitor coupled microstrip resonator band pass filter," *2015 IEEE Radio and Wireless Symposium (RWS)*, 2015.
5. Chiou, Y.-C. and G. M. Rebeiz, "Tunable 1.55–2.1 GHz 4-pole elliptic bandpass filter with bandwidth control and dB rejection for wireless systems," *IEEE Transactions on Microwave Theory and Techniques*, Vol. 61, No. 1, 117–124, 2013.
6. Stefanini, R., M. Chatras, and P. Blondy, "Compact 2-pole and 4-pole 1.5–0.9 GHz constant absolute bandwidth tunable filters," *2012 IEEE/MTT-S International Microwave Symposium Digest*, 2012.
7. Cao, L., J. Yan, and L. Yin, "A compact tunable dielectric filter with constant absolute bandwidth," *2018 International Conference on Microwave and Millimeter Wave Technology (ICMMT)*, 1–3, 2018.
8. Jung, D., J. N. Hansen, and K. Chang, "Piezoelectric transducer-controlled tunable hairpin bandpass filter," *Electronics Letters*, Vol. 48, No. 8, 1–2, 2012.
9. Al-Ahmad, M., R. Maenner, R. Matz, et al., "Wide piezoelectric tuning of LTCC bandpass filters," *IEEE MTT-S International Microwave Symposium Digest*, 1–4, 2005.

10. Hsieh, L.-H. and K. Chang, "Tunable microstrip bandpass filters with two transmission zeros," *IEEE Transactions on Microwave Theory and Techniques*, Vol. 51, No. 2, 520–525, 2003.
11. Cao, L.-Z. and L. X. Yin, "The implementation and design of piezoelectric transducer-tuned dielectric filter," *Acta Electronica Sinica in Chinese*, Vol. 45, No. 8, 1964–1969, 2017.
12. Cameron, R. J., "Advanced coupling matrix synthesis techniques for microwave filters," *IEEE Transactions on Microwave Theory and Techniques*, Vol. 51, No. 1, 1–10, 2003.
13. Thomas Brian, J., "Cross-coupling in coaxial cavity filters — A tutorial overview," *IEEE Transactions on Microwave and Techniques*, Vol. 51, No. 4, 1368–1376, 2003.